Lawrence Berkeley Laboratory
UNIVERSITY OF CALIFORNIA

Accelerator & Fusion Research Division

To be submitted for publication

SOME ASPECTS OF PLASMA TOMOGRAPHY

Rory Niland

January 1983

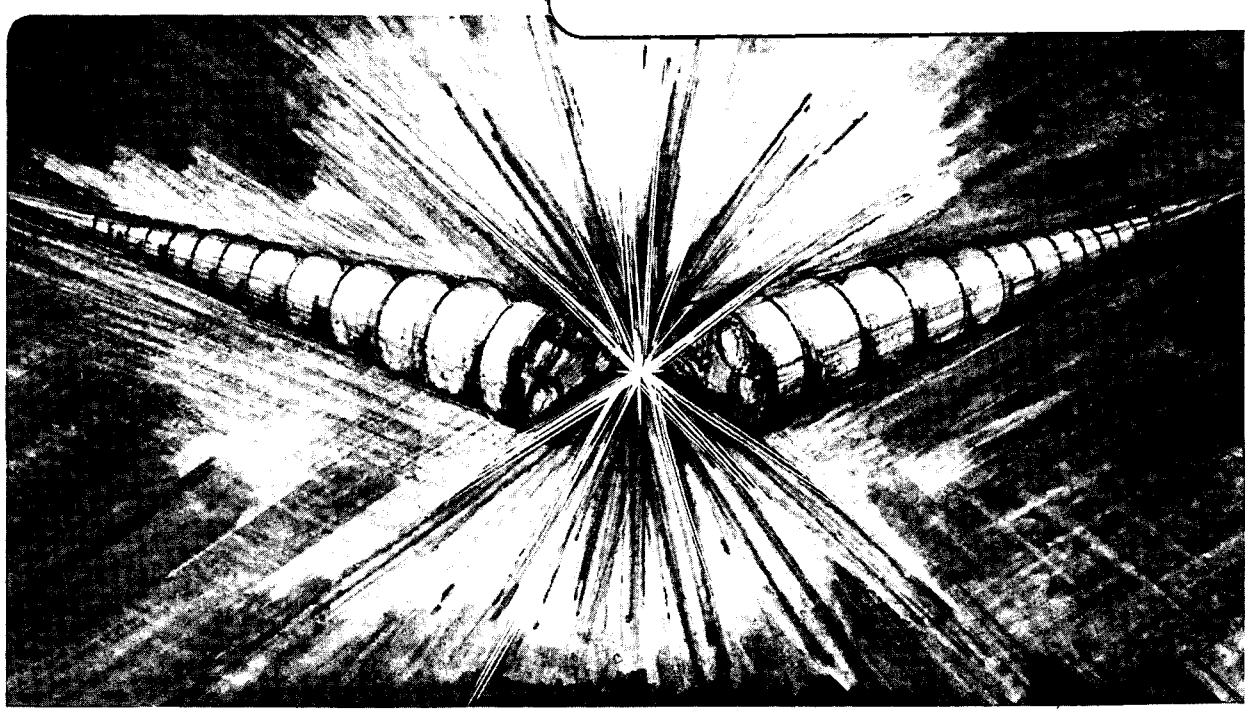

Prepared for the U.S. Department of Energy under Contract DE-AC03-76SF00098

DISCLAIMER

Some Aspects of Plasma Tomography*

Rory Niland†

Lawrence Berkeley Laboratory
University of California
Berkeley, CA 94720

Abstract

(A) m projections, equispaced in angle, of a two-dimensional object yield precisely m^2 real numbers characterizing the object. These are generalized moments of the object and are free of aliasing contamination. A reconstruction with minimal norm and matching those moments can be produced.

(B) If the object is discretized on an N x N grid then the minimal norm reconstruction which matches the m projections is most accurate for N approximately equal to m, i.e., is also characterized by about m^2 parameters.

---

* This work was supported by the Director, Office of Energy Research Office of Fusion Energy, Applied Plasma Physics Division, of the U.S. Department of Energy under Contract # DE-AC03-76SF00098.

† Present address: Wills Plasma Physics Department, University of Sydney, Sydney, Australia 2006.

Some Aspects of Plasma Tomography*

Rory Niland†

Lawrence Berkeley Laboratory
University of California
Berkeley, CA 94720

0. Introduction

Tomography, or the reconstruction of an object from its projections, has in the last few years been applied to plasma physics diagnostics. The differences from medical applications seem to be twofold: Because of the transient nature of plasma phenomena, all of the tomographic observations should be made simultaneously, in a single plasma shot. This demands considerable hardware. For this reason, and because of limited physical access to most machines, the number of 'views' or different angles of projection tends to be small, from 2 to perhaps 8. Secondly, in distinction to other uses of tomography where the interest is in revealing a particular object or structure clearly, in plasma applications typically we want reliable numbers, e.g. in the experiment of Myers and Levine (1978), intensities of the spectral line at various points inside the plasma; and to avoid spurious interpretations, it is necessary to have some estimate of the reliability of these reconstructed intensities. There exists a large number of reconstruction algorithms (Brooks and DiChiro 1976) and for the case of many views of a static object some are obviously to be preferred. For plasma applications the choice is much less clear.

* This work was supported by the Director, Office of Energy Research, Office of Fusion Energy, Applied Plasma Physics Division, of the U. S. Department of Energy under Contract No. DE-AC03-76SF00098.

† Present address: Wills Plasma Physics Dept., University of Sydney, Sydney, Australia 2006

The report is organized as follows: Section 1 gives some of the background that motivated this work, and summarizes numerical experiments on the behavior of the algebraic iterative algorithms. Section 2 is a presentation of what seems to me a very natural description of the reconstruction process, yielding some insight into its ultimate resolution, and what imposes the limits. Section 3 is a new algorithm which guarantees a reconstruction free of aliasing artefacts yet retains as many degrees of freedom as any algorithm can. Section 4 is a study of least-squares reconstructions in general.

I wish to acknowledge Booth Myers and Morton Levine for encouraging my initial interest in this work, and my colleagues at LBL for their support, in particular, Ben Feinberg and Ludmilla Soroka.

1.0. Background

This study was motivated by the experimental work of Myers and Levine (1978), who used 4-view tomography in an attempt to obtain spatially resolved spectroscopic measurements in a Tormac plasma. We summarize the relevant details here: The plasma whose expected shape is shown in Fig. 1 was contained in a glass vessel of rectangular cross section of dimensions 5 x 10 inches. Measurements were taken with a probe consisting of a collimating head attached to a long fiber optic leading to a 16 channel polychromator. In all, measurements were taken along 88 lines of sight belonging to projections at 0,45,90 and 135 degrees. In order to estimate noise, three plasma shots were taken at each position. The Algebraic Reconstruction Algorithm (ART) of Gordon et al. (1970) was used to reconstruct a 10 x 20 cell plasma.

As a preliminary, the algorithm was tested with various artificial intensity distributions considered typical, and seemed to perform adequately. However, it turned out later that this initial testing was not severe enough (Gilbert 1972); the reason is that the rays used as test data for ART were generated by summing intensity values at the centers of the cells, i.e. the object generating the data was already considered to be discretized. This so-called pseudo-projection data favors the ART algorithm (Colsher 1977). When instead, more realistically, a continuous test object was chosen and the ray values generated by analytic integration or accurate numerical integration, ART's performance was decidedly impaired, because it is sensitive to even slight inconsistency in the projections. Another drawback to this type of testing is the difficulty of creating a sufficiently large class of test objects, quantifying the algorithm's performance without too much subjectivity, and reaching generalizations by inspection. Next were considered for comparison the other algebraic (i.e. non-Fourier) algorithms: ILST (Gotein 1972) and SIRT (Gilbert 1972). The procedures are not described here since all of the algebraic algorithms are more or less implementations of a least squares solution to the discretized problem (for SIRT, see Lakshminarayanan (1976), and for ART, Herman, et. al. (1973)), and this is discussed in Section 4, where it is suggested that for a low number of views as is reasonable in plasma physics the best strategy may be to solve the LS problem directly, by the pseudoinverse matrix, not iteratively. Comparative tests of the three algorithms included:

1. Reconstruction of a sine wave of various frequencies and propagation directions, and doing a 2D Fourier analysis of the result, in an attempt to describe the processes as spatial filters.

2. Reconstruction of various made-up intensity distributions that mimicked the plasma shape, for example a hole in center and scalloped edge (Fig. 2).

3. Reconstructing an impulse function of intensity at various positions.

4. Varying the number of iterations and studying the norm of the difference between the reconstructed function and the true one.

5. Repeating a reconstruction 100 times with Gaussian noise on the input data and computing the mean and standard deviation in each cell of the reconstruction, and the correlation between cells.

6. Related to the last item, the effect of spatially averaging over blocks of cells of different sizes was studied.

Because these algorithms will be superseded by others described later in the paper, the results are described only briefly. ILST and SIRT amplify noise on the ray sums (integrals of intensity along the line of sight) considerably less than ART, which is important since experimental measurements will always have noise present. In addition they are more tolerant of slight inconsistency in the data than ART, and produce less correlation between neighboring cell values than ART, which by its nature tends to smear nearby values together. Low spatial correlation permits some noise reduction by grouping neighbors together.

The most important conclusion, however, is that the exact reconstructed intensity distribution is dependent on the choice of algorithm, the number of iterations, and the intensity distribution of

the object, in an unpredictable way. This is clearly unsatisfactory. All this work was done on the original 10 x 20 cell grid.

Finally, the question was addressed: Given a reconstructed intensity distribution, for example done by SIRT with 10 iterations, which overall seems about the best choice, what numbers can be extracted from it to prescribed accuracy- say ±10% or ±20% regardless of the original object, perhaps within a reasonable class of objects. For certainly the 200 individual cell values are unreliable; and certainly the mean intensity over the whole reconstruction is exact. What intermediate partitioning of the plasma vessel will yield reliable numbers?

The answer from numerical experiment is that if ±20% accuracy is required, the spatial resolution is quite low, corresponding to between 2 and 8 partitions of the vessel, or blocks of 5 x 5 to 10 x 10 of the original small cells. This result is in approximate agreement with the theoretical work of Klug and Crowther (1972) who use a Fourier formulation of tomographic reconstruction—described in the next section—and it can be made plausible by some simple descriptions of the process.

2.0. A theory of Tomographic Reconstruction

This section looks at a theoretical description of image reconstruction. It is essentially a recapitulation of the papers of Klug, Crowther, and DeRosier, and the central idea is that of expanding the object to be reconstructed into a set of basis functions, and noting that if a finite number m views are taken, only a finite number of the basis functions can be retrieved, the others being confused with each other by the mechanism of angular aliasing.

2.1. Projection Slice Theorem

Let $f(x,y)$ be a two dimensional intensity distribution (the "object"). Then the one dimensional Fourier transform of a projection of $f(x,y)$ at any angle is the slice at the same angle through the two dimensional Fourier transform of $f(x,y)$.

Sketch of Proof: The 2D Fourier transform is defined as

$$F_2[f(x,y)] = \iint f(x,y) e^{-2\pi i(xk_x + yk_y)} dx dy \qquad (2.1)$$

The projection of f onto the x-axis is

$$P(x) = \int f(x,y)\, dy$$

$$\therefore F_1[P(x)] = \int P(x) e^{-2\pi i x k_x} dx$$

$$= \iint f(x,y) e^{-2\pi i x k_x} dx dy$$

$$= [F_2 f](k_x, 0)$$

i.e. the slice of the spectrum along the k_x-axis. Since it is obvious or easily proved that

$$F_2 R_\theta f = R_\theta F_2 f$$

Where R_θ is a rotation operator, we see that any line through the origin can be rotated to the x-axis, thus proving the theorem.

2.2. Spatial Resolution

We follow the Klug and Crowther (1972) paper. The object $\psi(r,\theta)$ now expressed in polar coordinates, is contained within a circle of radius a so that

$$\psi = 0 \qquad \text{for} \qquad r > a$$

We expand ψ in an infinite series of basis functions whose 2D Fourier transforms may be calculated analytically. Then assuming m equispaced projections of ψ are given, we have m slices of the 2D spectrum $\Psi(\rho,\phi)$ from which we want to retrieve the amplitudes of as many of the basis functions as possible. An appropriate complete orthonormal set of basis functions on the disk are: (Courant and Hilbert 1953)

$$\begin{aligned} \psi_{ns}(r,\theta) &= \alpha_{ns}^{-1} e^{in\theta} J_n(2\pi R_{ns} r) \qquad r \leq a \\ &= 0 \qquad\qquad\qquad\qquad\qquad\quad r > a \end{aligned} \tag{2.2}$$

Here R_{ns} is the s'th root of $J_n(2\pi R_{ns} a) = 0 \quad s = 1,2,3,....$

and J_n is the n'th order Bessel function. The class of functions which can be thus expanded is given in Lebedev (1972) or Watson (1952).

We write

$$x_{ns} = 2\pi R_{ns}$$

α_{ns} normalizes ψ_{ns} so that

$$\int_0^a r dr \int_0^{2\pi} d\theta \; |\psi_{ns}|^2 = 1$$

Thus

$$\alpha_{ns} = a\sqrt{\pi} J'_n(x_{ns} a)$$

$$= \mp a \sqrt{\pi} J_{n\pm 1}(x_{ns} a)$$

It is straightforward to show that the inner product

$$(\psi_{ns}, \psi_{n's'}) = \int_0^a r dr \int_0^{2\pi} d\theta \, \psi^*_{ns} \psi_{n's'} = \delta_{nn'} \delta_{ss'}$$

The object is expanded as

$$\psi(r,\theta) = \sum_{n=0}^{\infty} f_n(r) e^{in\theta}$$

$$= \sum_{n=0}^{\infty} \sum_{s=1}^{\infty} q_{ns} \psi_{ns}$$

where the real part of the right-hand side is understood. The inversion of this relation may be performed by

$$f_n(r) = \frac{1}{2\pi} \int_0^{2\pi} \psi(r,\theta) e^{-in\theta} d\theta$$

and from the standard properties of Bessel functions (Mathews and Walker 1970)

$$q_{ns} = (\psi, \psi_{ns}) = \frac{-2\sqrt{\pi}}{a} \int_0^a f_n(r) J_n(x_{ns} r) r dr$$

The 2D Fourier transform of the object

$$F_2[\psi(r,\theta)] = \Psi(\rho,\phi)$$

may be expressed as an expansion in the functions Ψ_{ns} where (Goodman 1968)

$$\Psi_{ns}(\rho,\phi) = F_2[\psi_{ns}(r,\theta)]$$

$$= \alpha_{ns}^{-1} e^{in(\phi-\frac{\pi}{2})} 2\pi \int_0^a J_n(x_{ns} r) J_n(2\pi\rho r) r dr \quad (2.3)$$

$$= e^{in(\phi-\frac{\pi}{2})} \frac{R_{ns} J_n(2\pi\rho a)}{\sqrt{\pi}(\rho^2 - R_{ns}^2)}$$

at the point $\rho = R_{ns}$ the function is continuous and may be written

$$e^{in(\phi-\frac{\pi}{2})} a\pi J_n'(x_{ns} a)$$

$$= \alpha_{ns} e^{in(\phi-\frac{\pi}{2})}$$

Because the Ψ_{ns} are Fourier transforms of an orthogonal set of functions they have the property that $\Psi_{ns}(R_{ns'}, \phi)$ vanishes for all s' except s' = s, where it has amplitude α_{ns}. Hence

$$\Psi(R_{ns},\phi) = \sum_n q_{ns}\, \alpha_{ns} e^{in(\phi-\frac{\pi}{2})}$$

so that

$$q_{ns} = \frac{1}{2\pi\alpha_{ns}} \int_0^{2\pi} \Psi(R_{ns},\phi) e^{-in(\phi-\frac{\pi}{2})}\, d\phi \qquad (2.4)$$

This is a prescription for extracting the coefficient of a basis function from the 2D Fourier transform of the object.

2.3 Angular Aliasing

Assume now that the m equispaced views of the object are given, for concreteness at

$$\theta = (k-1)\pi/m \qquad k = 1,2,\ldots,m$$

where we have taken by convention $\rho > 0$. Thus there are 2m values of ϕ at which $\Psi(\rho,\phi)$ is known.

By Shannon's sampling theorem, or more clearly by graphical inspection, we may see that we can distinguish only the azimuthal variations

$$\cos \ell\theta \qquad \ell = 0,1,2,\ldots m$$

$$\sin \ell\theta \qquad \ell = 1,2,\ldots m-1$$

All higher components are aliased down into this range, so that

$$\ell = 2m \pm p,\ 4m \pm p,\ 6m \pm p,\ldots$$

all appear as $\ell = p$ and cannot be identified as high frequencies. Thus the finite angular sampling makes it impossible to retrieve any ψ_{ns} with $n \geq m$.

Even for $n < m$, ψ_{ns} with high s, those basis functions with high radial frequency, cannot be retrieved because of another mechanism which is best illustrated by an example: Take $m = 4$ views. To find the amount of the basis function Ψ_{13} in the object measure the amplitude of $e^{i\phi}$ at $\rho = R_{13}$ in the spectrum Ψ. By virtue of equation (2.4) none of Ψ_{1s} $s = 1,2,\ldots$ $(s \neq 3)$, contribute at this value of ρ. However, aliased-down functions like Ψ_{7s} $s = 1,2,\ldots$ all contribute as can be seen from equation (2.3). In particular Ψ_{71} and Ψ_{13} are of comparable magnitude at $\rho = R_{13}$, so are inextricably mixed as far as 4-view tomography is concerned. The best strategy then seems to exclude Ψ_{13} deliberately from the reconstruction. This 'contamination' of basis functions of low order n by aliased-down basis functions of high n is the process which converts a limit in angular sampling to a limit in spatial resolution.

From equation (2.3) it can be shown that, for $m = 4$, the only uncontaminated and therefore fully retrievable basis functions are

$$\Psi_{01,02,11,21}$$

ψ_{03} and ψ_{12} have 34 % and 24 % admixture of higher functions (assuming all basis functions are present and of equal amplitude) and are perhaps marginal. The rest must be excluded. Consequently the maximum spatial frequency $\rho_{max} = R_{21}$ (or R_{12}) i.e. about 1/a and the resolution distance

$$\frac{1}{2\rho_{max}} \cong \frac{a}{2}$$

although resolution is an ill-defined quantity for tomography with few views.

Notice also, with m = 4, that four complex functions ψ_{ns} are reliably retrieved so that approximately 8 parameters referring to the object can be claimed.

In section 3, by optimum choice of the basis functions, two improvements are made to this theory: The number of retrievable parameters for m equidistant views is extended in all cases to m^2; and a set of retrievable functions is found which has no aliasing contamination at all.

2.4. Intuitive Derivations of the Resolving Power of Tomography

This and the next section give simple-minded models of the limits of spatial resolution of m-view tomography.

Suppose the object is a sinusoidal wave travelling in the θ direction so that

$$f(x,y) = \sin(xk_x + yk_y)$$

where

$$k_x = 2\pi\rho\cos\theta, \quad k_y = 2\pi\rho\sin\theta$$

also let it vanish outside the disk of radius a; then its Fourier transform has the form

$$\frac{J_1(2\pi\delta/a)}{\delta/a}$$

where δ is the distance from the point (ρ,ϕ). For the object to be seen via its projections, one of the m slices must cut the transform. A marginal condition for that is

$$\frac{0.61}{a} > \rho \sin \frac{\pi}{2m}$$

which means that the least visible wave, one whose k-vector bisects the angle between two views, is on the threshold of being detected. For $m = 4$, this criterion gives $\rho_{max} = 1.47/a$. Klug and Crowther's more realistic estimates correspond to the slices seeing about 1/3 of the height of the spectral peak.

Derivation in Real Space

Consider the same object and suppose it is enclosed now in the square $0 \leq x, y \leq 2a$. The projection onto the x-axis is

$$P(x) = \int_0^{2a} f(x,y)dy$$

$$= 2a \sin (xk_x + ak_y) \frac{\sin ak_y}{ak_y}$$

The degree of modulation, or 'visibility' of p(x) as x varies is

$$\frac{P_{max} - P_{min}}{P_{max} - P_{min}} = \frac{\sin ak_y}{ak_y}$$

It is 100% for $ak_y = 0$ (i.e. $\theta = 0$ or $\lambda \to \infty$) and falls to zero at $ak_y = \pi$. Hence a threshold condition for detectability of the object is

$$\lambda = \frac{1}{\rho} > 2a \sin\theta$$

The least favorable value of θ is $\frac{\pi}{2m}$ so that $\lambda > 2a \sin \frac{\pi}{2m}$.
Notice that the two criteria more or less agree.

3.0. Alias Free Algorithm

The Bessel functions in which the object was expanded in Section 2 were chosen arbitrarily. Klug and Crowther (1972) say that similar results are found if the prolate spheroidal functions are used instead. We are interested in this section in the property of tomographic reconstruction that is being manifested here, independent of the choice of basis functions.

Let us expand the object (presumed zero outside of a circle of unit radius) as

$$\psi(r,\theta) = \frac{1}{2} a_0(r) + \sum_{\ell=1}^{\infty} (a_\ell(r)\cos\ell\theta + b_\ell(r)\sin \ell\theta) \qquad (3.1)$$

It is less confusing to write the formulas in terms of real quantities although sometimes complex expressions will be used for

conciseness. The projection in the direction ϕ of a function $f(r)e^{i\ell\theta}$ is (see Fig. 3)

$$\int_{s=-\sqrt{1-t^2}}^{s=+\sqrt{1-t^2}} f(r)e^{i\ell\theta}d\theta$$

$$= \int_t^1 \frac{f(r)rdr}{\sqrt{r^2-t^2}}\left\{e^{i\ell(\phi+\frac{\pi}{2}+\cos^{-1}\frac{t}{r})} + e^{i\ell(\phi+\frac{\pi}{2}-\cos^{-1}\frac{t}{r})}\right\}$$

$$= A_\ell[f(r)]e^{i\ell(\phi+\frac{\pi}{2})}$$

where the operator A_ℓ is defined by

$$A_\ell[f(r)] = g(t) = 2\int_t^1 \frac{f(r)T_\ell(t/r)rdr}{\sqrt{r^2-t^2}} \qquad (3.2)$$

and $T_\ell(x)$ is a Chebyshev polynomial of the first kind

$$T_\ell(x) = \cos(\ell\cos^{-1}x) \qquad 0 \leq x \leq 1$$

$$= \cosh(\ell\cosh^{-1}x) \qquad 1 < x < \infty$$

It is well known (Cormack 1964, Sneddon 1972, Deans 1977) that the integral equation(3.2) can be inverted, yielding $f(r)$ for given $g(t)$. Although the inversion formula is very ill-conditioned and unsuitable for numerical calculations, the method of inversion is useful: Notice that (3.2) has the form of Mellin convolution, i.e. if the variables were changed by

$$r = e^{\rho}, \qquad t = e^{\tau}$$

it would become an ordinary convolution. Following Sneddon, write (3.2) as

$$g(t) = \int_0^{\infty} f_1(r) K_1(t/r)\, dr/r$$

where

$$f_1(r) = 2rf(r)H(1-r)$$

$$K_1(u) = \frac{T_{\ell}(u)}{\sqrt{1-u^2}} H(1-u)$$

$H(u)$ is the Heaviside function, $= 0 \quad u < 0$

$$1 \quad u \geq 0$$

Then defining the Mellin transformation

$$M[g(t)] = \int_0^{\infty} g(t) t^{s-1} dt$$

where s is complex with a real part such as to make the integral converge, we have

$$M g = (M f_1)(M K_1)$$

or

$$\int_0^1 g t^{s-1} dt = \int_0^1 f r^s dr \times 2 \int_0^1 \frac{T_{\ell}(r) r^{s-1} dr}{\sqrt{1-r^2}}$$

write now $s = k+1$ $(k = 0,1,2,\ldots)$ and use Sneddon's form for MK_1 to obtain

$$\int_0^1 g(t)t^k dt = \Gamma_{\ell k} \int_0^1 f(r)r^k r dr \tag{3.3}$$

where

$$\Gamma_{\ell k} = \frac{\pi}{2^k} \frac{\Gamma(k+1)}{\Gamma(\frac{k-\ell+2}{2})\,\Gamma(\frac{k+\ell+2}{2})} \tag{3.4}$$

An important consequence is that, if $k + \ell$ is even and $k < \ell$ then $\Gamma_{\ell k} = 0$. Hence, regardless of the function $f(r)$, $g(t) = A_\ell f$ has zero k'th moments for k satisfying the above conditions. This fact will be used to make a reconstruction algorithm free of aliasing.

For general values of k and ℓ, $\Gamma_{\ell k}$ may be evaluated using the relations

$$\Gamma(z+1) = z\,\Gamma(z)$$
$$\Gamma(1/2) = \sqrt{\pi}.$$

3.1. Avoiding Aliasing

Aliasing enters because the object is viewed from a finite number of different angles. Suppose for the moment we have an infinite number of different views of the object (3.1). The projection data then form a continuum of values

$$G(t,\phi) \qquad 0 \le t \le 1, \qquad 0 \le \phi < 2\pi$$

From the definition of A_ℓ we see that

$$G(t,\emptyset) = \frac{1}{2}A_0 a_0(r) + \sum_{\ell=1}^{\infty} (A_\ell a_\ell(r)\cos \ell(\phi + \tfrac{\pi}{2}) + A_\ell b_\ell(r)\sin \ell(\phi + \tfrac{\pi}{2}))$$

A reconstruction procedure would involve retrieval of $g_\ell(t) = A_\ell f_\ell$ by Fourier analysis:

$$g_\ell(t) = A_\ell(a_\ell + ib_\ell) = \frac{1}{\pi}\int_0^{2\pi} G(t,\phi)e^{i\ell(\phi + \frac{\pi}{2})}\, d\phi \qquad (3.5)$$

and then

$$f_\ell(r) = A_\ell^{-1} g_\ell$$

using some method.

In the case of finite views m, the Fourier integral (3.5) becomes the discrete Fourier transform (DFT)

$$g(t) = \frac{1}{2m}\sum_{k=1}^{2m} G(t,\phi_k)e^{i\ell(\phi_k + \frac{\pi}{2})} \qquad (3.6)$$

where (assuming now equispaced views)

$$\phi_k = (k-1)\pi/m \qquad k = 1,2,\ldots 2m.$$

It may be verified that instead of yielding g for a given value of ℓ, this formula yields a linear combination of g_ℓ and $g_{\ell'}$, where ℓ' ranges over the set of aliases of ℓ:

$$\ell' = 2m \pm \ell, \quad 4m \pm \ell, \ \ldots \qquad (3.7)$$

It is possible to excise all the contamination of g_ℓ from the higher aliasing terms $g_{\ell'}$. What moments of $g_{\ell'}$ vanish? The k'th moment vanishes if $k + \ell'$ is even and $k < \ell'$. Take $\ell' = 2m-\ell$ for definiteness; then the vanishing moments are

$$\ell \text{ even:} \quad k = 0,2,4,\ldots 2m-\ell-2$$
$$\ell \text{ odd:} \quad k = 1,3,5,\ldots 2m-\ell-2$$

Notice also that these same moments are zero for $g_{\ell'}$ where $\ell' = 2m+\ell$, and also for all of the higher aliased values of ℓ.

Thus although we have by the DFT obtained a function g(t) which is not the desired $g_\ell(t)$, because of aliasing, yet we do know some of its moments unambigously.

By virtue again of (3.4), some of the lower moments of g_ℓ itself are zero; so that there is a range

$$k = \ell,\ \ell + 2, \ell + 4,\ldots 2m-\ell-2 \qquad (3.8)$$

for ℓ even or odd, of non-zero alias-free moments of g_ℓ, $m-\ell$ altogether, obtainable from g(t) the result of the DFT (3.6).

3.2. Construction of the Algorithm

We wish to exclude the aliased information from g(t) and also to avoid the ill-conditioned process A_ℓ^{-1}. These goals can be achieved together.

Suppose for some fixed ℓ we have performed a DFT on the data $G(t,\phi_k)$ and have g(t) - a mixture of g_ℓ and its aliases. We can

extract the m-ℓ reliable moments of g_ℓ. Now find the function $\overline{f}_\ell(r)$ such that $\overline{f}_\ell(r)$ has the correct m-ℓ moments and

$$\int_0^1 |\overline{f}_\ell|^2 r dr \qquad \text{is minimal.}$$

This is motivated by a principle of parsimony. Other measures might also be used; for example maximizing entropy (Frieden 1975) and this is considered in Section 3.4.

The problem has a simple geometric formulation: Define an inner product on [0,1] as

$$(f,g) = \int_0^1 fg\, r dr \tag{3.9}$$

Then we are given the moments of $\overline{f}_\ell$

$$\begin{aligned} \int_0^1 g(t) t^k dt &= \Gamma_{\ell k} \int_0^1 \overline{f}_\ell(r) r^k r dr \\ &= \Gamma_{\ell k}(\overline{f}_\ell, r^k) \end{aligned} \tag{3.10}$$

The other constraint becomes $(\overline{f}_\ell, \overline{f}_\ell)$ is minimal. It is easy to see that the solution is: $\overline{f}_\ell$ lies in the subspace spanned by

$$\{r^k\} \quad k = \ell,\ \ell+2,\ \ell+4, \ldots 2m-\ell-2 \tag{3.11}$$

and its projections on to those spanning functions are given by equation (3.10). This may also be phrased as $\bar{f}_\ell$ has the form

$$\alpha_1 r^{\ell} + \alpha_2 r^{\ell+2} + \ldots + \alpha_{m-\ell} r^{2m-\ell-2} \tag{3.12}$$

and the coefficients are determined from equation (3.10).

Because of the formulation in terms of moments, ill-conditioned Hilbert matrices will naturally appear in the solution of the above. However, for few views the problem is not intrinsically ill-conditioned. A suitable procedure to avoid the Hilbert matrices is to span the subspace (3.11) by a set of functions $\{\phi_\mu(r)\}$ (a different set for each m and ℓ) orthonormal with respect to the metric (3.9). They may be generated, for example, by the Gram-Schmidt process. Then compute the numbers $(\bar{f}_\ell, \phi_\mu)$, $\mu = 1,2,3,\ldots$ whence

$$\bar{f}_\ell(r) = \sum_{\mu=1}^{m-\ell} (f_\ell, \phi_\mu)\phi_\mu \tag{3.13}$$

It is convenient to take

$$g(t) = \delta(t-t_0)$$

and generate the corresponding $\bar{f}_\ell(r)$. Then it is easy to extend to the case of an arbitrary sampled g(t).

3.3. Summary of the alias-free algorithm

Given: real projection data $G(t,\phi_k)$. Compute 'contaminated' $g_\ell(t)$ by the DFT equation (3.6). Calculate the m-ℓ correct moments of g_ℓ. Compute the minimal functions $\bar{f}_\ell$ of the form (3.12). Then the reconstructed alias free object is

$$\frac{1}{2} a_0(r) + \sum_{\ell=1}^{m-1} (\bar{a}_\ell(r)\cos \ell\theta + \bar{b}_\ell(r)\sin\ell\theta) \qquad (3.14)$$

3.4. Maximum Entropy Formulation

Rather than seek the function $\bar{f}_\ell(r)$ whose projection $A_\ell\bar{f}_\ell$ has the correct moments, we may search for a function $f(r)$ ($= a_\ell(r), b_\ell(r)$ separately) which maximimizes the entropy

$$H = -\int f(r) \ell n\ f(r) dr$$

and generates the correct moments (Jaynes 1968). The solution is

$$f(r) = \exp(\sum_k \lambda_k r^k)$$

where $k = \ell, \ell+2, \ldots 2m-\ell-2$ and the real constants λ_k are determined by the moment constraint (3.10). This may involve a search rather than solution in closed form. Notice that f is now constrained to be positive, which may lead to difficulties in the presence of noise. This algorithm has not been investigated by me.

There exists another reconstruction based on maximizing entropy (Minerbo 1979), in which, however, the constraint is the given set of projections, not the selected alias-free moments.

3.5. A More General View

Sections 3.0 and 3.1 establish this result: tomography with m equispaced views yelds m^2 reliable numbers referring to the object $\psi(r,\phi)$ and these numbers may be identified as generalized moments of ψ:

$$Q_{\ell k} = \int_0^{2\pi} d\theta \; e^{i\ell\theta} \int_0^1 r \, dr \, r^k \, \psi(r,\theta) \qquad (3.15)$$

where $\ell = 0, 1, \ldots,$ and k is given (3.8). For example for m = 4 the m^2 real weighting functions are

$\ell = 0$:	1	r^2	r^4	r^6
$\ell = 1$:	r	r^3	r^5	x $\sin\theta$, $\cos\theta$
$\ell = 2$:	r^2	r^4		x $\sin 2\theta$, $\cos 2\theta$
$\ell = 3$:	r^3			x $\sin 3\theta$, $\cos 3\theta$

A number of lines of investigation will now be sketched out. We particularly want to impose the physical constraint $\psi \geq 0$ which is not done in sections 3.2 - 3.4.

(a). Since $\psi \geq 0$ (3.15)is a two dimensional extension of the classical moment problem (Shohat and Tamarkin 1943) and it may be possible to extract information about the solution space of ψ. This approach does not attempt to construct an 'image' of ψ, but rather to use the information gained by tomography to, for example, resolve conflicting hypotheses.

(b). To obtain an image (3.15) might be discretized in r and θ and treated as a quadratic programming problem.

$$\text{minimize } \iint \psi^2 \, r\,dr\,d\theta$$
$$\text{subject to } \psi \geq 0$$
$$\text{and the } m^2 \text{ constraints of (3.15).}$$

(c). Very appealing, given its robust properties, is a maximum entropy solution $f(r,\theta)$ which is naturally positively constrained and satisfies the generalized moment conditions (3.15). Standard methods (Minerbo 1979) show that the f which maximizes

$$\iint r\,dr d\theta\, f \ln f \tag{3.16}$$

has the form

$$f = \exp \sum_{i=1}^{m^2} \lambda_i W_i (r,\theta) \tag{3.17}$$

where the W_i are the above weight functions and the Lagrange multipliers λ_i are adjusted to satisfy (3.15). Although in principle the nonlinear system may be solved by a Newton-Raphson method, in practice difficulties arise even for m = 4, and it is somewhat easier to convert to an optimization problem and adjust $\underset{\sim}{\lambda}$ to minimize the squared error in satisfying (3.15). The BFGS algorithm (Stoer and Bulirsch 1980) was used for these tests with some success for $m \leq 4$.

(d). A variant of (c) is to forgo the special form (3.17) and after discretizing the problem in r and ϕ attempt to maximize entropy subject to the conditions (3.15). The problem becomes:

$$\text{minimize} \quad \Sigma f_i \, \ell n \, f_i$$
$$\text{subject to } f_i \geq 0$$
$$\text{and } A \underset{\sim}{f} = \underset{\sim}{Q}$$

Where A is an m x n matrix ($m \geq n$) and $\underset{\sim}{Q}$ is the vector of observed moments. Minerbo (1979) refers to an ART-like algorithm for this problem.

4.0. Least Squares Reconstruction: Introduction

In this section we study least squares reconstruction which is what many of the unconstrained algebraic reconstruction algorithms aspire to. Suppose the object f(x,y) is contained now within a square $0 \leq x,y \leq 1$ and we are given its projections in two, four, or more directions. The problem is to find the function $\bar{f}(x,y)$ such that $\bar{f}(x,y)$ has the correct projections in the given directions and

$$\iint_0^1 dxdy(f-\bar{f})^2 \qquad \text{is minimum}$$

This is equivalent also to minimizing

$$\iint \bar{f}^2 dxdy \tag{4.1}$$

i.e. finding the smoothest object which has the observed projections (Shepp and Kruskal 1978). Notice that even if $f \geq 0, \overline{f}$ is not constrained to be positive.

In order to use the language of linear algebra, discretize the square into N x N equal small squares or cells. Then the object is represented by a vector $\underset{\sim}{\xi}$ of dimension N^2.

This section contains a geometrical description of LS reconstruction, explicit formulas for the case of 2 and 4 equispaced views, and most importantly, a demonstration that if N is increased beyond about the number of views no further information is gained, and in fact the reconstruction departs further and further from the true object. This essentially means that LS reconstruction, like the alias free algorithm, yields a reconstructed object characterized by about m^2 real parameters.

4.1. Geometric Description of Least Squares Reconstruction

From the discretized object $\underset{\sim}{\xi}$ generate the set of 'ray sums', i.e. line integrals through the object by

$$\underset{\sim}{b} = A \underset{\sim}{\xi} \tag{4.2}$$

where $A_{ij} = 1$ if cell j contributes to ray i, and is zero otherwise. For m = 2 views for example, A is a $2N \times N^2$ matrix so that the system is certainly underdetermined for N > 2. However, such a system always has a unique minimal solution x such that x is the vector of least norm satisfying Ax = b. As in the last section this choice is motivated by the desire to assume as little as possible about the underdetermined solution. This minimal solution may be conveniently written in terms of the Moore-Penrose Pseudoinverse of the matrix A (Noble and Daniel 1977)as

$$\underset{\sim}{x} = A^{+}\underset{\sim}{b}$$

A^{+} is characterized algebraically by the relations

$$\begin{aligned} (A^{+}A)^{T} &= A^{+}A \\ (AA^{+})^{T} &= AA^{+} \\ AA^{+}A &= A \\ A^{+}AA^{+} &= A^{+} \end{aligned} \qquad (4.3)$$

It may also be defined by the limits (Nashed 1976)

$$\begin{aligned} A^{+} &= \lim_{\varepsilon \to 0^{+}} (A^{T}A + \varepsilon I)^{-1}A^{T} \\ &= \lim_{\varepsilon \to 0^{+}} A(AA^{T} + \varepsilon I)^{-1} \end{aligned}$$

Showing that it reduces to the ordinary inverse for a non-singular matrix. More useful for calculation is the expression of A^{+} in terms of the singular value decomposition (SVD) of A. An arbitrary matrix A (M x N) may be decomposed as

$$A = USV^{T}$$

where U is an orthogonal matrix (M x N), V is orthogonal (N x N) and S is diagonal

$$S = \text{diag}(\sigma_1, \sigma_2, \ldots \sigma_r, 0, 0, \ldots 0)$$

where r is the rank of A. Then

$$A^+ = VS^+U^T \tag{4.4}$$

where

$$S^+ = \text{diag}(\sigma_1^{-1},\sigma_2^{-1},\ldots\sigma_r^{-1},0,0,\ldots 0)$$

Consider now the matrix A^+A which 'images' the true object $\underset{\sim}{\xi}$ into its LS reconstruction x. It is a projection operator since

$$(A^+A)^2 = A^+(AA^+A) = A^+A$$

by the Moore-Penrose relations. More explicitly, using the SVD,

$$A^+A = VS^+SV^T$$

$$S^+S = \text{diag}\,(\underbrace{1,1,\ldots 1}_{r},0,0\ldots 0) = M \text{ (say)}$$

so $$\underset{\sim}{x} = A^+A\underset{\sim}{\xi} = VMV^T\underset{\sim}{\xi}$$

and

$$V^T\underset{\sim}{x} = MV^T\underset{\sim}{\xi}$$

Thus relative to the new basis which consists of the row vectors of V

$$\underset{\sim}{x}' = M\,'\underset{\sim}{\xi}$$

i.e. the operator makes zero the last N-r elements of $\underset{\sim}{\xi}'$.

A^+A projects $\underset{\sim}{\xi}$ onto the space spanned by the rows of A. This rowspace may also be written $R(A^T)$ - the range of A^T- since it consists of all vectors of the form $A^T\underset{\sim}{u}$ (arbitrary $\underset{\sim}{u}$). It is also the subspace which consists of all possible back projections (in the

real world!) as may be seen from the following:

$$A^{+} = A^{T}(AA^{T})^{+}$$

This may be readily proved from the SVD of A (Lawson and Hanson 1974) Thus

$$\underset{\sim}{x} = A^{+}\underset{\sim}{b} = A^{T}(AA^{T})^{+}\underset{\sim}{b} = A^{T}\underset{\sim}{c} \qquad (4.5)$$

where

$$\underset{\sim}{c} = (AA^{T})^{+}\underset{\sim}{b}$$

so that $\underset{\sim}{x}$, the LS reconstructed image, is the back projection of a vector $\underset{\sim}{c}$ derived from the vector of observed ray sums $\underset{\sim}{b}$. For the simplest case of two views at right angles $\underset{\sim}{x}$ is just the back projection of $\underset{\sim}{b}$ together with a constant offset (see next section). For $m > 2$, however, there does not seem to be any intuitively satisfying relationship between $\underset{\sim}{b}$ and $\underset{\sim}{c}$. This is also remarked upon by Logan and Shepp (1975) who show analogously to the above that the minimal function generating the correct projections can be expressed as a sum of 'ridge functions.'

4.2. Two View Tomography

Suppose we view the discretized square in the x and y projections only, so that there are 2N observations and N^2 unknowns. In this simple case A^{+} and $A^{+}A$ may be written down explicitly. For example

$N^2A^{+}A =$

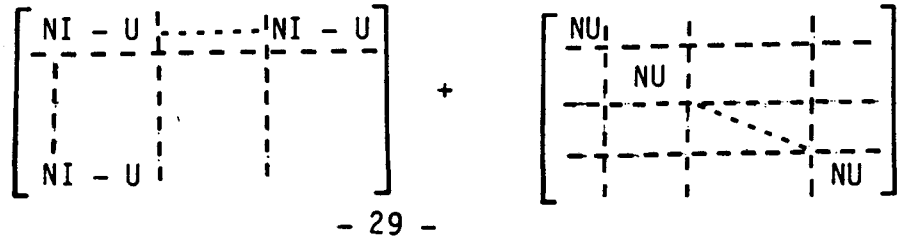

where $U_{ij} = 1$ $(i, j = 1,2,\ldots,N)$ and I is the unit N x N matrix. Letting $N \to \infty$ reveals the continuous form of the operator. It is given by

$$\overline{f}(x,y) = \int f dx + \int f dy - \iint f dx\, dy$$

from which it is clear (perhaps contrary to first thought) that the only functions perfectly retrievable from two views are of the form

$$f(x,y) = f_1(x) + f_2(y)$$

It is of interest that the numerical computation of the SVD of A for two views - which used the algorithm given by Forsythe, Malcolm and Moler (1977) - showed that the rank of A was 2N-1. This might be expected since the sum of observations in each view must be equal, so reducing the number of independent measurements by one. In practice the redundant measurement might serve as a check of the consistency of the data.

4.3. Four View Tomography

The matrix A, now of dimensions $6N-2 \times N^2$, is set up by the formulas in Fig. 4. The SVD algorithm gives rank (A) = 6N-9, indicating 7 hidden relationships between the rays. The system (4.2) is thus determinate only for $N < 3$. For $N = 4$ there are 15 independent equations in 16 unknowns. An attempt was made to discern the form of A^+ and A^+A as $N \to \infty$, but it was not successful. A complicating factor is that the SVD algorithm encounters numerical problems for N greater than 5 or 6. However, there exist other interative methods, in particular the method of Kaczmarz (which is also the basis of ART). It

is lucidly discussed by Tanabe (1971). The algorithm is (supposing A is NR x NC and $\underset{\sim}{a}_i^T$ is the i'th row of A)

For j = 1 to NR

$\underset{\sim}{x} = 0$

for iteration = 1 to 10 (or test)

for i = 1 to NR

$$\beta = (\underset{\sim}{a}_i^T \underset{\sim}{x} - \delta_{ij}) / \underset{\sim}{a}_i^T \underset{\sim}{a}_i$$

for k = 1 to NC

$$x_k = x_k - \beta A_{ik}$$

next k

next i

next iteration

for i = 1 to NC

$$A^+_{ij} = x_i$$

next i

next j

to generate A^+A change NR in the first line to NC, and the Kronecker delta to A_{ij}.

It seems a good idea to use a stored A^+ to perform LS reconstruction if there are only a few views. This avoids the usual vagaries of deciding when to terminate the iterative algorithm. The noise properties can also be thoroughly understood.

4.4. Error in Least Squares Reconstruction

Referring to Fig. 5 we see that an object $f(x,y)$ may be projected into the two orthogonal subspaces $N(A)$ and $R(A^T)$ (assuming $N \to \infty$) as

$$f = f_o + f_1$$

$N(A)$ is the space of 'invisible objects' so that $Af_o = 0$, and $R(A^T)$ is the space of back projections as before, so that $f_1 = A^T u$, for some function u. The LS reconstruction of f is f_1 and the error is f_o. We want to study

$$\iint f_o^2 \, dx\,dy$$

or more exactly, the discretized approximation to it

$$S_N = N^2 \sum_{j=1}^{N^2} \left(\int_{\text{cell } j} f_o \, dx\,dy \right)^2 \qquad N = 1,2,3,... \qquad (4.6)$$

If N is small enough to determine the problem, $S_N = 0$. It would be nice to prove that S_N increases monotonically with N above this critical value. Although this is not rigorously true it is a strong trend: for an arbitrary function $g(x,y)$ - not necessarily in the space of invisible functions - we have

$$S_{kN} \geq S_N \qquad k = 1,2,3,...; \text{ all } N$$

The proof is illustrated for k = 2. Suppose a given cell of size 1/N x 1/N has integrals over its quarters of a,b,c,d, (Fig. 6) then

$$S_N = \left(\frac{a+b+c+d}{4}\right)^2$$

$$S_{2N} = 4\left(\left(\frac{a}{4}\right)^2 + \left(\frac{b}{4}\right)^2 + \left(\frac{c}{4}\right)^2 + \left(\frac{d}{4}\right)^2\right)$$

Now we have $S_{2N} \geq S_N$ by Schwartz' inequality.

However, it is not true for an arbitrary function that S_N is monotonically increasing as counterexamples may be readily found.

Extensive numerical experimentation was done: the unit square was divided into 60 x 60 cells and the value of S_N computed for N = 1,2,3,4,5,6,10,15,30,60 for a great variety of trial functions g. For g a polynomial in x,y of degree 5 or less, in 250 trials with coefficients randomly chosen from a uniform distribution on [-1,1], the monotonicity of the sequence $\{S_N\}$ was never violated. At the other extreme a very 'rough' function was constructed by assigning a random number from the same distribution to each of the 3600 cells of the square. Now about one trial in five showed a non-monotonic sequence, however, in all cases monotonicity would have been restored by increasing just one S_N, usually S_3 or S_4. It is interesting that this 'rough' case can perhaps be properly analyzed by statistical methods - forming the distribution function of S_N for each N.

These results, which have not included the fact that the error function is 'invisible' illustrate the strong trend of S_N to increase monotonically with N.

The conclusion is that if N is taken small enough to make the problem determined, the error of LS reconstruction is zero (apart from error in assuming that the object is discretized). If N is increased above this, to obtain 'higher resolution,' the error of the reconstruction most likely increases, although for some special objects it may not and these permit somewhat higher resolution.

4.5. Practical Details

If there are m views about m^2 detectors will be used. It is desirable that the field of view of a detector is compatible with the size of the discretized cells: nothing is gained by needle beams. It is not necessary that the detectors be evenly spaced; they can be fanned, or their beams overlap. The only requirement is that the linear system of equations relating the detector signals to the cell values is determinate (or nearly so). Any too great license with the geometry will manifest in a large condition number for the matrix A, indicating that the detector signals are not sufficiently independent. Hence, given the geometry, the first step is to set up the linear system of equations. This can be readily computerized by dividing the cells again very finely and automatically counting the number of small cells in the overlap of each large cell and ray. The next step is to compute the SVD of the matrix, and inspect the spectrum of singular values, to ensure the effective rank of A is adequate. Finally, the pseudoinverse of A is formed and stored.

5.0. Conclusions

Two algorithms for tomographic in construction have been described: the first, motivated by the work of Klug and Crowther (1972), reconstructs the smoothest object whose projections agree with the observed projections only in those moments known to be immune to aliasing. This object is characterized by precisely m^2 parameters, where m is the number of (equispaced) views. The form of the object is given in equation (3.14), where each of the functions $a_\ell(r)$ and $b_\ell(r)$ is a linear combination of

$$\{r^k\} \quad k = \ell,\ \ell+2,\ \ell+4,\ldots 2m-\ell-2.$$

It should be pointed out that the reconstruction will not in general have the same projections as the original object.

The second algorithm is a least squares method to find the smoothest object that generates the observed projections. For small m it is conveniently written in terms of a pseudoinverse matrix formed once and for all for a given geometry, rather than by applying iterative methods to the data. It was shown that the region in which the object lies should be discretized sufficiently coarsely to ensure a determined problem. Generally this means, for an N x N grid, that N is about m or a little less, depending on the rank of the projection matrix A in the actual experimental setup.

Two comments may be made about the LS method: first, the object is considered to be a set of cells with uniform intensity in each cell. The goodness of this approximation cannot be judged without knowing the geometrical setup of the detectors. For example, if m = 2 and the

detectors collect only light from complete cells, as in the idealized two view case treated, there will be no error and the cell values in the reconstruction will be the true integrals of the object over the cell area. On the other hand with 4 views and detector 'rays' of finite width some of the cells will be in two different rays and the relation between the reconstructed value and the true integral depends on the exact geometry. Secondly, there is no problem of aliasing since that is essentially deferred to the end, to the experimenter's judgement. For example, if the object is sin 7θ which is indistinguishable with 4 views from sin θ, the cells will contain after reconstruction the correct 2D integrals of sin 7θ (neglecting the discretization error for now), and the reconstruction will look like a sin θ object. The experimenter must bear in mind that it could be one of the higher aliases. In contrast the alias-free algorithm will return a zero object in this case since it only accepts the azimuthal variations of equation (3.14) and none of these are present.

Notice also that the LS algorithm produces a (perhaps crudely) discretized object and the alias-free algorithm a smooth one. On the other side, although both reconstructions are parametrized by m^2 numbers, the LS reconstruction requires only m^2 lines of sight, and the other prefers, in order to estimate the moments with precision, a continuum or finely sampled projection at each angle. This is not usually a problem.

6.0. References

Brooks, R. A., and DiChiro, G., Review Article: "Principles of Computer Assisted Tomography in Radiographic and Radiosotopic Imaging," Phys. Med. Biol. 21 689-732 (1976).

Colsher, J. G. "Iterative 3D Image Reconstruction from Tomographic Projections," Computer Graphics and Image Processing, 6 543 (1977).

Cormack, A. M., J. Appl. Physics 35 2908 (1964).

Courant, R., and Hilbert, D., Methods of Mathematical Physics, Vol. I, Interscience Publishers, N. Y. (1953).

Crowther, R. A., Derosier, D. H. Klug, A., Proc. Roy. Soc. 317 319 (1953).

Deans, S. R., "The Radon Transform: Some Remarks and Formulas for Two Dimensions," Lawrence Berkeley Laboratory Report LBL-5691 (1977).

Forsythe, G. E., Malcolm, M. A., and Moler, C. B., Computer Methods for Mathematical Computations, Prentice Hall (1977).

Frieden, B. R., Image Enhancement and Restoration, in Picture Processing and Digital Filtering, Topics in Applied Physics, Vol. 6, Springer (1975).

Gilbert, P., "Iterative Methods for the 3D reconstruction of an Object from Projections," J. Theor. Biol. 36, 105 (1972).

Goodman, J. W., Introduction to Fourier Optics, McGraw-Hill, San Francisco, Ca (1968).

Gordon, R., Bender, R., and Herman, G. T., J. Theor. Biol. 29, 471 (1970).

Gotein, M., "3D Density Reconstruction from a Series of 2D Projections," Nucl. Instrum. and Methods. 101, 509 (1972).

Herman, G. T., Lent, A., and Rowland, S. W., "ART: Mathematics and Applications," J. Theor. Biol. 42, 1-32 (1973).

Jaynes, E. T., IEEE Trans. Syst. Sci. Cybern. SSC-4, 227 (1968).

Klug, A., and Crowther, R. A., "3D Image Reconstruction from the Viewpoint of Information Theory," Nature 238, 435 (1972).

Lakshminarayanan, A. V., and Lent, A., "SIRT as a Least-Squares Method," SPIE, Vol. 96, Opt.Instrum. in Medicine V (1976).

Lebedev, N. N., Special Functions and Their Applications, Dover, N.Y. (1972).

Logan, B. F., and Shepp, L. A., "Optimal Reconstruction of a Function from its Projections," Duke Math. J. 42, 645 (1975).

Luke, Y. L., Mathematical Functions and Their Approximations, Academic Press (1975).

Mathews, J., and Walker, R. L., Mathematical Methods of Physics, 2nd edition, Benjamin, N. Y. (1970).

Myers, B. R., and Levine, M. A., "2D Spectral Line Emission Reconstruction as a Plasma Diagnostic," Rev. Sci. Inst. 49, 610 (1978).

Minerbo, G., "MENT: A Maximum Entropy Algorithm for Reconstructing a Source from Projection Data," Computer Graphics and Image Processing 10, 48 (1979).

Nashed, M. Z., Perturbations and Approximations for Generalized Inverses and Linear Operator Equations, in "Generalized Inverses and Applications," Ed. M. Z. Nashed, Academic Press (1976).

Noble, B., and Daniel, J. W., Applied Linear Algebra, Prentice-Hall (1977).

Shepp, L. A., and Kruskal, J. B., "Computerized Tomography: The New Medical X-Ray Technology," Amer. Math. Monthly 85, 420 (1978).

Shohat, J.A., and Tamarkin, J.D., The Problem of Moments, Amer. Math. Soc. Monographs, (1943).

Sneddon, I., The Use of Integral Transforms, McGraw-Hill (1972).

Stoer, J., and Bulirsch, R., Introduction to Numerical Analysis, Springer (1980).

Strang, G., Linear Algebra and its Applications, Academic Press, N. Y. (1976).

Tanabe, K. "Projection Method for Solving a Singular System of Linear Equations and its Applications," Numer. Math. 17, 203 (1971).

Watson, G. N., A Treatise on the Theory of Bessel Functions, Cambridge University Press (1952).

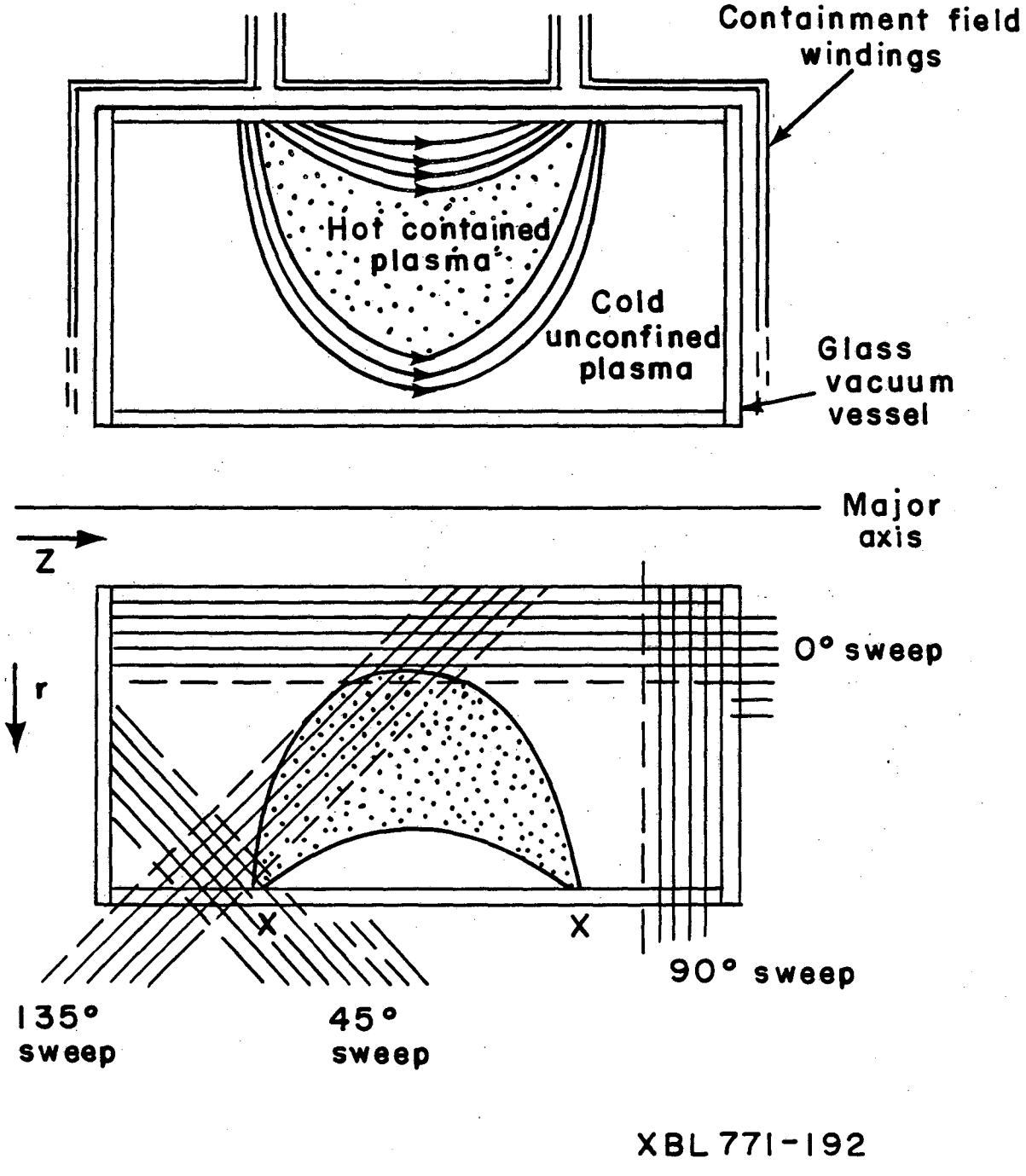

Figure 1. Tomography on the Tormac IV plasma source (Myers & Levine 1978).

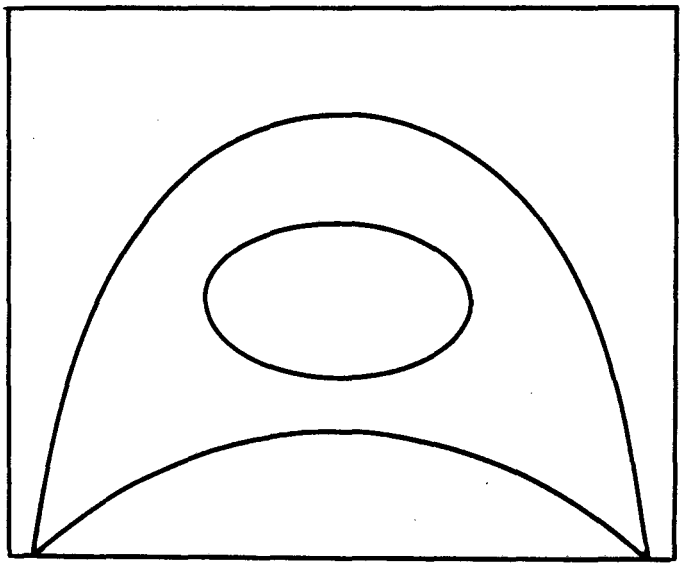

Figure 2. A test object simulating the expected intensity distribution of the Tormac plasma.

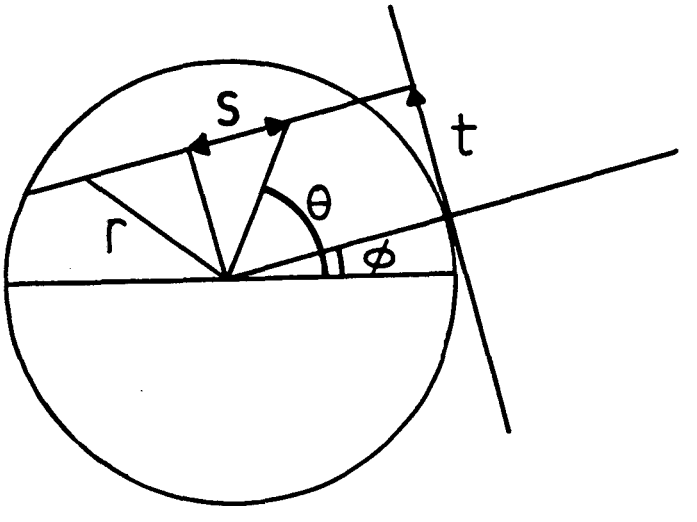

Figure 3. Geometry for the definition of the operator A_ℓ.

XBL 8111-12626

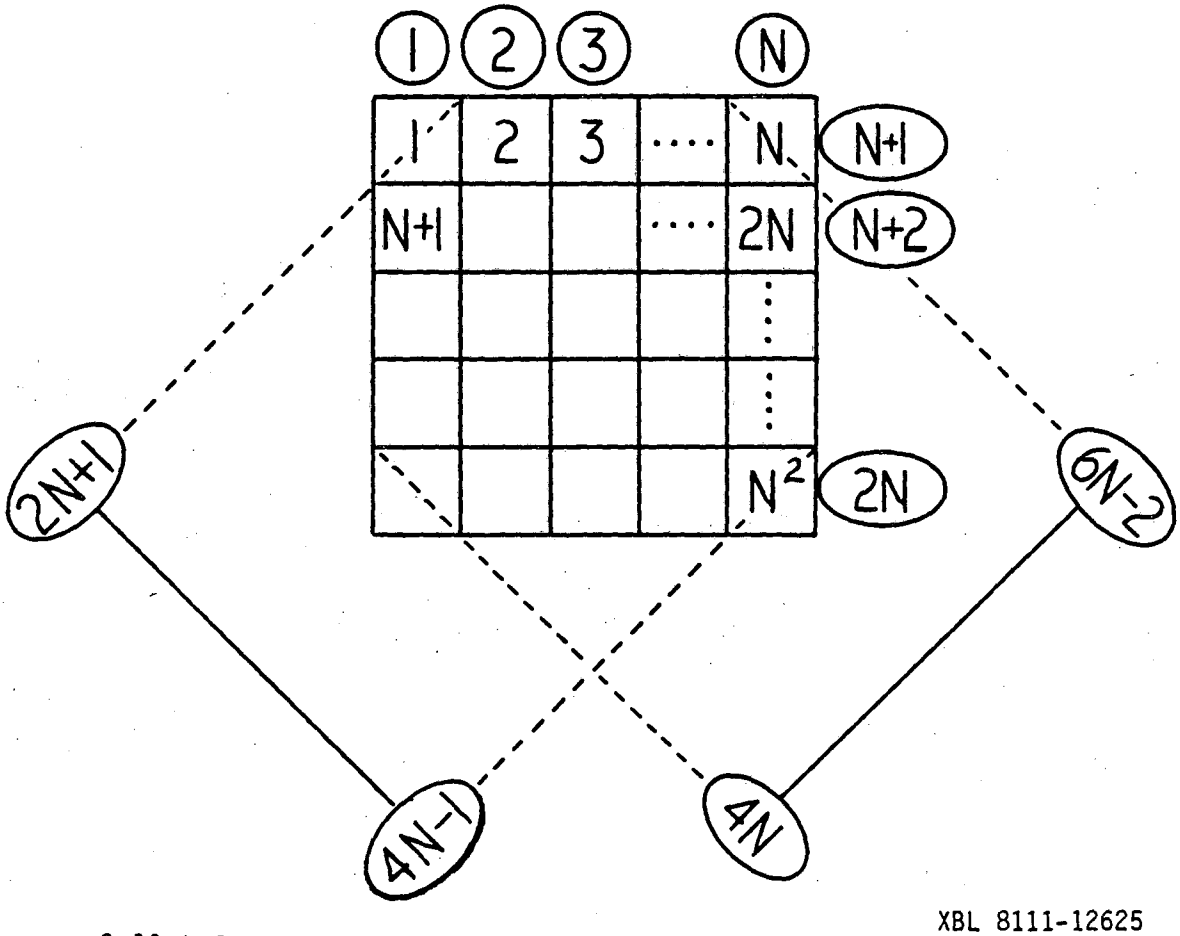

XBL 8111-12625

Cell k lies on rays

$\ell_1 = 1 + \text{mod}(k-1,N) = \nu$

$\ell_2 = 1 + \text{int}\left(\frac{k-1}{N}\right) + N = \mu + N$

$\ell_3 = 2N + \mu + \nu - 1$

$\ell_4 = 5N + \mu - \nu - 1$

Figure 4. Four view tomography

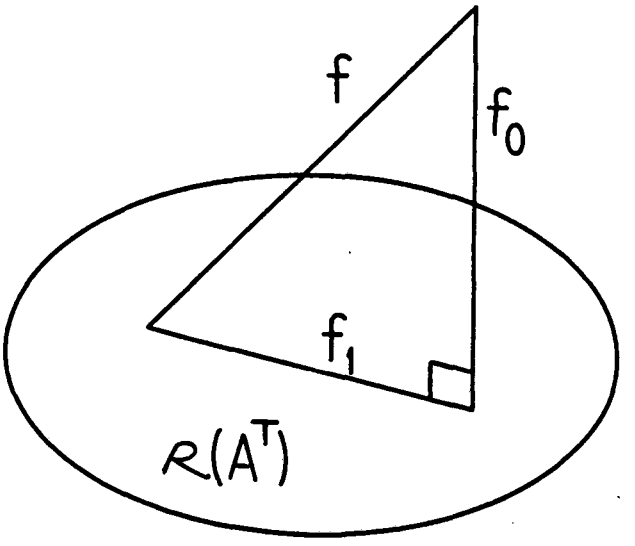

Figure 5. Any object can be decomposed into a back projection plus an "invisible object."

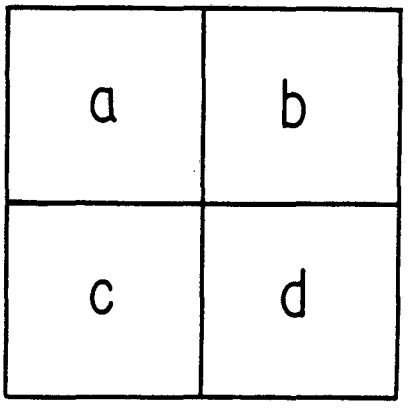

XBL 8111-12624

Figure 6. (Used in Section 4.4).

TECHNICAL INFORMATION DEPARTMENT
LAWRENCE BERKELEY LABORATORY
UNIVERSITY OF CALIFORNIA
BERKELEY, CALIFORNIA 94720